In vivo photosensitizer tomography inside the human prostate

Johan Axelsson,[1,*] Johannes Swartling,[2] and Stefan Andersson-Engels[1]

[1]*Department of Physics, Lund University, P.O. Box 118, SE-221 00 Lund, Sweden*
[2]*SpectraCure AB, Ole Römers väg 16, SE-223 70 Lund, Sweden*
**Corresponding author: johan.axelsson@fysik.lth.se*

Received October 7, 2008; revised November 28, 2008; accepted November 29, 2008;
posted December 8, 2008 (Doc. ID 102292); published January 21, 2009

Interstitial photodynamic therapy (IPDT) provides a promising means to treat large cancerous tumors and solid organs inside the human body. The treatment outcome is dependent on the distributions of light, photosensitizer, and tissue oxygenation. We present a scheme for reconstructing the spatial distribution of a fluorescent photosensitizer. The reconstruction is based on measurements performed in the human prostate, acquired during an ongoing IPDT clinical trial, as well as in optical phantoms. We show that in an experimental setup we can quantitatively reconstruct a fluorescent inclusion in a fluorescent background. We also show reconstructions from a patient showing a heterogeneous distribution of the photosensitizer mTHPC in the human prostate.

OCIS codes: 170.3880, 170.3660, 170.5180, 170.7230.

Interstitital photodynamic therapy (IPDT) is a promising treatment alternative or complement to radition therapy of solid tumors. As of today several research groups have focused on treating prostate cancer using IPDT, where optical fibers are implanted into the prostate gland [1–3]. The fibers deliver therapeutic light, i.e., light that activates the photosensitizing drug, resulting in the generation of radicals. The radicals will then react with the tissue leading to necrosis. To target the entire prostate gland, commonly the approach in prostate-photodynamic therapy (PDT), as well as localized regions, rigorous dosimetry is required.

Current schemes adopt an explicit dosimetry model [4] and rely only on the light fluence as a measure of the PDT dose [5,6]. It has been reported that by adjusting the light dose based on pretreatment monitoring of the photosensitizer concentration, interpatient variation of the treatment outcome can be reduced [7]. The same should hold for intrapatient variations. With knowledge also of the photosensitizer concentration further improvements may be possible. Hence there is a need for methods that assess the spatial distribution of the photosensible drug. Futhermore these methods form the foundation for spatial reconstruction of the bleaching kinetics during treatment. Potentially such methods could render an improved light-photosensitizer dosimetry model.

In this Letter we present a scheme that is capable of reconstructing an estimate of the spatial distribution of a photosensitizer within the human prostate. The reconstruction is based on data acquired during our ongoing clinical trial of primary prostate cancer. The IPDT instrument operates along the scheme depicted in Fig. 1. PDT treatment is governed by 18 optical fibers that are coupled through a fiber switch to 18 diode lasers. The lasers emit at 652 nm matching the absorption peak for mTHPC, the photosensitizer employed. During treatment the light irradiation is halted, and a sequence of measurements is performed. Here each of the fibers emit light, while the six neighboring fibers collect the transmitted and fluorescent light. Light detection is governed by a set of spectrometers. For this Letter the important measurable is the mTHPC fluorescence emitted as a broad peak between 710 and 730 nm following excitation at 652 nm. Further details about the predecessor to the system working along the same scheme can be found in [8]. The main differences between the present system and the predecessor is the number of available fibers and the operating wavelength now optimized for mTHPC. The currently employed dosimetry algorithm is explained in [5]. During a monitoring sequence a total of 108 fluorescence recordings are acquired between 54 source-detector pairs. The fibers are positioned within the prostate gland with the intention to maximize the light dose within the prostate while surrounding tissues are spared. The optimal positions are found using a random search algorithm [5]. The algorithm relies on the knowledge of the three-dimensional anatomy of the prostate and surrounding tissues, retrieved from a transrectal ultrasound scan.

The fluorophore distribution is represented by the fluorophore yield $\eta(\mathbf{r}) = \gamma\mu_{af}(\mathbf{r})$, where γ is the quantum yield and $\mu_{af}(\mathbf{r})$ is the absorption coefficient for the fluorophore. The problem at hand is to find an estimate of the fluorophore yield that minimizes the residual between a forward model calculated for η and the measurements. This minimization problem is ill-posed, thus regularization is incorporated. Here we employ Tikhonov regularization so that the minimization problem becomes

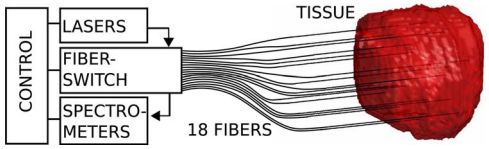

Fig. 1. (Color online) Schematic picture of the IPDT instrument.

$$\Omega = \arg\min_{\eta}(\|\delta(\eta)\|^2 + \lambda\|L[\eta - \eta_0]\|^2). \quad (1)$$

Here $\delta(\eta)=\Gamma - F(\eta)$, where $F(\eta)$ is the forward model calculated for parameter η, while Γ denotes the measurable; λ is the regularization parameter, and L is a regularization matrix, explained below, while η_0 is the initial estimate of the fluorophore distribution, here set to zero.

The forward model employed is the diffusion equation [9]. The measurable is the fluorescence measurement scaled with the excitation measurement, normally referred to as the normalized Born ratio [10]. Discretizing the geometry into elements, defined by nodes, the forward model is given by

$$F(\eta) = \frac{1}{U_x(r_s,r_d)}\sum_{n=1}^{NN} U_m^*(r_d,r_n)U_x(r_s,r_n)\Delta V \eta_n, \quad (2)$$

where $r_{s,d,n}$ denotes the coordinates for source, detector, and internal node, respectively. $U_{x,m}$ represents the forward solution of the excitation light and fluorescent light, respectively, while $U^*_{x,m}$ is the adjoint solution to the forward fluorescent problem. Further NN is the total number of nodes, ΔV is the element volume, and η_n is the fluorescence yield for node n. In this Letter the forward solutions ($U_{x,m}$) are retreived using homogeneous optical properties. The inverse problem is solved using an iterative scheme. The parameter estimate for iteration i is denoted as η_i. To find the parameter η_i that minimizes Eq. (1) the first-order derivative is set to zero, i.e., $\partial\Omega/\partial\eta=0$. In matrix notation this leads to [11]

$$\frac{\partial\Omega}{\partial\eta} = J^T\delta(\eta_i) - \lambda L^T L[\eta_i - \eta_0] = 0. \quad (3)$$

Here J denotes the Jacobian defined by $J=\partial F/\partial\eta$. Using a Taylor series to linearize the forward model in Eq. (3), i.e., $F(\eta_i)\approx F(\eta_{i-1})+J[\eta_i-\eta_{i-1}]$, the parameter update equation becomes

$$\eta_i = \eta_{i-1} + (J^TJ + \lambda L^TL)^{-1}\times[J^T\delta(\eta_{i-1}) - \lambda L^TL\eta_{i-1}]. \quad (4)$$

Calculations were performed using the NIRFAST package implementing the finite element method [12].

The regularization matrix follows the same scheme as presented in [11,12]. L is then a $[NN\times NN]$ matrix defined by $L_{i,j}=1$ if $i=j$, $L_{i,j}=0$ if i and j are not within the same tissue region, and $L_{i,j}=-1/\mathrm{NR}$ if i and j are different but in the same region. Here NR is the number of nodes in this region. The specific regions are defined through the sensitivity, i.e., Jacobian, where the sum of the Jacobian for all source-detector pairs is first calculated through $S_n=\Sigma_i^{NM}J_{i,n}$. The first region is formed by all nodes satisfying the criterion $S_n/\max(S)>0.05\%$, while the other region is formed by all the other nodes. The regularization parameter is chosen according to the L-curve method, where the solution norm $\|L\eta_\lambda\|$ is plotted versus the residual norm $\|F(\eta_\lambda)-\Gamma\|$ for a wide range of regularization parameters λ [13]. This is effectively done using a generalized singular-value decomposition of the matrix pair (J,L) thoroughly described in [13].

The ability of the reconstruction scheme to assess a fluorophore distribution within a scattering volume was verified employing data from an optical phantom experiment. The phantom was made of a plastic tank filled with Intralipid (Fresenius Kabi, 200 mg/ml) and ink (Pelican Fount India Ink, 1:100 stock solution). In the plastic tank a smaller container was placed filled with the same bulk phantom solution depicted in Fig. 2(d). Using a time-of-flight spectroscopy system [14], the bulk optical properties were assessed to be $\mu_a=0.058\ \mathrm{mm}^{-1}$ and $\mu_s'=0.95\ \mathrm{mm}^{-1}$ at 660 nm. The laser dye Oxazine-1 was used as the fluorophore. The quantum yield for Oxazine-1 is 0.11 [15]. The quantum yield was scaled to the wavelength range between 695 and 705 nm according to Eq. (16) in [16]. In the larger tank the fluorophore was mixed with the bulk solution in a concentration retrieving a fluorophore absorption coefficient of $\mu_{af}=3.9\times10^{-3}\ \mathrm{mm}^{-1}$. In the smaller compartment a higher concentration was used, yielding an absorption of $\mu_{af}=6.1\times10^{-3}\ \mathrm{mm}^{-1}$. Fiber positions were based on patient data from the clinical trial. The forward model was solved on a mesh made in COMSOL MULTIPHYSICS with a higher node density close to the fiber positions. The forward mesh consisted of 15,127 nodes, while the inverse problem was solved on a regular grid made of 3375 nodes after interpolating the forward solution onto the grid.

In Figs. 2(a)–2(c) the reconstructed fluorophore absorption coefficient is seen. In Figs. 2(a) and 2(b) the smaller compartment is reconstructed within 15% of the true absorption coefficient as seen in Fig. 2(d). The absorption coefficient in the container is lower, although it is overestimated by approximately 40%. This is an effect inherited by the region-based prior that adds smoothing to the result, and hence the result is effectively averaged within each region. This results in a lower contrast between the smaller compartment and the container. In Figs. 2(a)–2(c) it is also seen that the fluorophore absorption is very low outside the prostate. This is also an effect of the

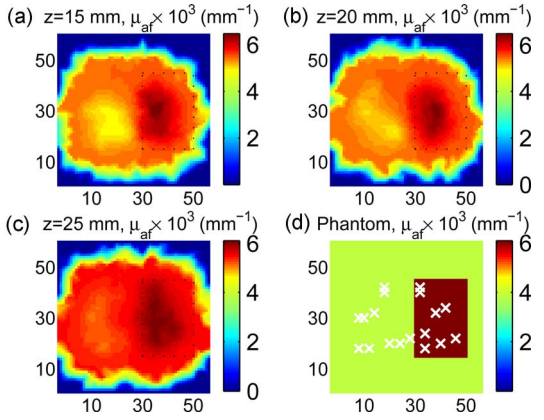

Fig. 2. (Color online) (a)–(c) Reconstruction results from a phantom experiment showing cross-sectional slices at $z=15$, 20, and 25 mm, respectively. (d) Schematic of the phantom fluorophore distribution. The fiber positions in the xy plane are also shown.

region-based prior that is formed based on the sensitivity. Outside the prostate the sensitivity is low owing to fiber positioning. Figure 2(c) shows a decreased fluorescent contrast between the compartment and the background. This is consistent with the low number of optical fibers positioned deeper in the volume.

Data acquired during a prostate-PDT session within the scope of our ongoing clinical trial of primary localized prostate cancer were used to reconstruct the mTHPC distribution in the human prostate. Data were collected 96 h postdrug injection. The reconstruction results are shown as cross-sectional slices in Figs. 3(a)–3(c). Optical properties for the human prostate were assessed using spatially resolved measurements described in [5]. In Fig. 3(d) the different regions used in the region-based regularization matrix is seen in one cross-sectional slice. The mTHPC distribution depicted in Figs. 3(a) and 3(b) has a slight heterogeneous appearance. The distribution is smooth, which is expected owing to the region-based smoothing. The distribution is on the same scale as previously reported for another photosensitizer [17]. Figure 3(c) shows again a decreased contrast owing to the limited number of fibers deeper in the prostate, where the gland has a smaller diameter. The drug is administered 4 days prior to the treatment; hence it is expected that the drug has diffused out from the blood stream yielding a smooth drug distribution within the prostate.

The results presented here are initial reconstructions based on clinical as well as experimental data. It is seen that the fluorophore concentration is slightly overestimated. We believe that this effect is a result of the regularization scheme adopted in this Letter. Despite that the regularization smooths the solution, it is still possible to demarcate a region with higher fluorophore contrast in a three-dimensional volume. To improve the accuracy of the reconstruction method we are investigating alternative regularization schemes. Currently we are adopting this scheme to reconstruct changes in the fluorophore concentration in each voxel of the prostate tissue during a prostate-PDT treatment.

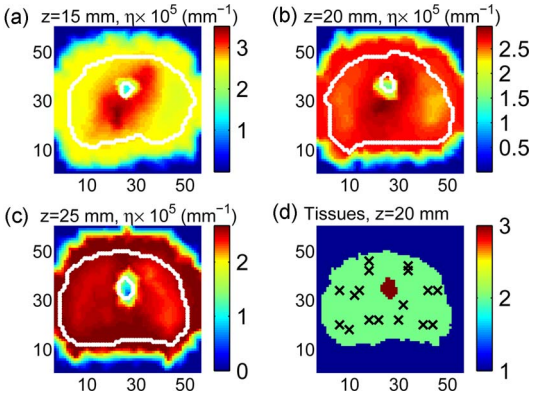

Fig. 3. (Color online) (a)–(c) Reconstruction results from a clinical trial showing cross-sectional slices at $z = 15$, 20, and 25 mm, respectively. White curves mark the prostate and urethra boundaries. (d) One slice of the prostate showing the tissue regions where 1 is normal, 2 is the prostate, and 3 is the urethra. The fiber positions in the xy plane are also shown.

This work was supported by SpectraCure AB.

References

1. K. L. Du, R. Mick, T. Busch, T. C. Zhu, J. C. Finlay, G. Yu, A. G. Yodh, S. B. Malkowicz, D. Smith, R. Whittington, D. Stripp, and S. M. Hahn, Lasers Surg. Med. **38**, 427 (2006).
2. C. M. Moore, T. R. Nathan, W. R. Lees, C. A. Mosse, A. Freeman, M. Emberton, and S. G. Bown, Lasers Surg. Med. **38**, 356 (2006).
3. R. A. Weersink, A. Bogaards, M. Gertner, S. R. H. Davidson, K. Zhang, G. Netchev, J. Trachtenberg, and B. C. Wilson, J. Photochem. Photobiol. B **79**, 211 (2005).
4. B. C. Wilson, M. S. Patterson, and L. Lilge, Lasers Med. Sci. **12**, 182 (1997).
5. A. Johansson, J. Axelsson, S. Andersson-Engels, and J. Swartling, Med. Phys. **34**, 4309 (2007).
6. M. D. Altschuler, T. C. Zhu, J. Li, and S. M. Hahn, Med. Phys. **32**, 3524 (2005).
7. X. D. Zhou, B. W. Pogue, B. Chen, E. Demidenko, R. Joshi, J. Hoopes, and T. Hasan, Int. J. Radiat. Oncol. Biol. Phys. **64**, 1211 (2006).
8. M. Soto-Thompson, A. Johansson, T. Johansson, S. Andersson-Engels, S. Svanberg, N. Bendsoe, and K. Svanberg, Appl. Opt. **44**, 4023 (2005).
9. S. R. Arridge, Inverse Probl. **15**, R41 (1999).
10. V. Ntziachristos and R. Weissleder, Opt. Lett. **26**, 893 (2001).
11. P. K. Yalavarthy, B. W. Pogue, H. Dehghani, and K. D. Paulsen, Med. Phys. **34**, 2085 (2007).
12. B. A. Brooksby, "Combining near infrared tomography and magnetic resonance imaging to improve breast tissue chromophore and scattering assessment," Ph.D. dissertation (Dartmouth College, 2005).
13. P. C. Hansen, Numer. Algorithms **6**, 1 (1994).
14. E. Alerstam, S. Andersson-Engels, and T. Svensson, Opt. Express **16**, 10440 (2008).
15. R. Sens and K. H. Drexhage, J. Lumin. **24**, 709 (1981).
16. J. Axelsson, J. Svensson, and S. Andersson-Engels, Opt. Express **15**, 13574 (2007).
17. J. C. Finlay, T. C. Zhu, A. Dimofte, D. Stripp, S. B. Malkowcz, T. M. Busch, and S. M. Hahn, Photochem. Photobiol. **82**, 1270 (2006).